

1           **BUCKLING OF BEAMS AND COATINGS OF FINITE WIDTH IN BILATERAL**  
2           **FRICTIONLESS CONTACT WITH AN ELASTIC HALF-SPACE**

3  
4                           Daniele BARALDI<sup>a</sup>, Nerio TULLINI<sup>b</sup>

5           <sup>a</sup> corresponding author; Università IUAV di Venezia, Italy; e-mail: danielebaraldi@iuav.it

6           <sup>b</sup> Department of Engineering; University of Ferrara, Italy; e-mail: nerio.tullini@unife.it

7   **ABSTRACT**

8       In this work, a simple and efficient finite element-boundary integral equation coupling method is  
9   adopted for studying the buckling of beams and coatings resting on a three-dimensional elastic half-  
10   space. For this purpose, a mixed variational formulation based on the Green function of the  
11   substrate is adopted by assuming as independent fields beam displacements and contact pressures.  
12   Euler-Bernoulli beams with finite width and different combinations of end restraints are considered.  
13   Some numerical tests illustrate the accuracy of the proposed formulation, with particular attention to  
14   the convergence to existing analytical and numerical solutions and to the proposal of new estimates  
15   of beams and coatings buckling wavelength and critical loads for varying length-to-width ratio and  
16   beam-substrate relative stiffness.

17   **KEYWORDS**

18       Beam; Coatings; Buckling; Transversely isotropic elastic half-space; Boussinesq solution;  
19   Frictionless bilateral contact; Mixed variational principle.

20   **1. INTRODUCTION**

21       The buckling of beams resting on an elastic substrate, soil, or foundation is a research topic that  
22   involves many engineering fields and it was studied in the past by many researchers. In the civil  
23   engineering field, examples of this problem are the buckling of highway or aircraft concrete  
24   pavements. In this context, the pioneering works of Wieghardt (1922) and Prager (1927) are based

25 on the assumption that the beam is resting on a continuously distributed set of springs (Winkler,  
26 1867). However, the actual response at the interface between the beam and the substrate is very  
27 difficult to be determined; hence, many foundation models can be found in literature for  
28 approximating the actual foundation behaviour (Selvadurai, 1979a). The first analytical approach  
29 for solving the problem of a beam on a semi-infinite elastic medium was performed by Biot (1937),  
30 who studied the bending of an infinite beam resting either on a two- or three-dimensional elastic  
31 half-space. In the same year, Reissner (1937) studied the stability problem of an infinite beam  
32 resting on a two-dimensional elastic support, whereas some decades later Murthy (1973) adopted  
33 Biot results for comparing the buckling of continuously supported beams on two- and three-  
34 dimensional half-space, showing the effect of a foundation extending beyond the width of the beam.

35 After the first pioneering works, the problem of a beam on elastic substrate, with particular  
36 attention to its stability, grew motivated by early structural problems of sandwich panels in  
37 airplanes (Allen, 1969). In particular, Gough et al. (1940) extended Biot and Reissner results of a  
38 beam on two-dimensional elastic half-space by considering various conditions of contact between  
39 the infinite beam and the half-plane. Further research activities on sandwich elements continued up  
40 to recent years (Ley et al., 1999; Davies, 2001) and also the buckling of concrete pavements and  
41 welded rails was studied (Kerr, 1974; Kerr, 1978; Kerr, 1984; Lim et al., 2003).

42 Recently, the stability of a beam on elastic half-space has been taken into consideration for the  
43 analytical and numerical simulation of the buckling of thin films on compliant substrates, and the  
44 research has been driven by developments in electronic industry (Shield et al. 1994; Bowden et al.,  
45 1999; Volynskii et al., 2000), with particular reference to stretchable electronic interconnects and  
46 devices (see Jiang et al. (2008) and references cited therein). The case of buckling without  
47 delamination is often called wrinkling (Genzer and Groenewold, 2006). In this field, the adoption of  
48 a beam model, in particular an Euler-Bernoulli one, on an elastic half-space is justified by the  
49 thickness of the support, which is often four order of magnitude larger than the film thickness.  
50 Furthermore, the contact is assumed to be frictionless, namely allowing a horizontal slip between

51 the film and the support, since it was demonstrated that the tangential tractions at the interface  
52 between the film and the compliant substrate has a negligible effect on the buckling of the system  
53 (Huang, 2005).

54 Considering microelectronic devices, the mechanical properties of thin films can be estimated by  
55 observing buckling patterns (Stafford et al., 2004; Wilder et al., 2006), and the buckling wavelength  
56 and amplitude are important for stretchable and flexible electronics. Many mechanical models have  
57 been developed in recent years (Huang and Suo, 2002a; Huang and Suo, 2002b; Stafford et al.,  
58 2004; Huang, 2005; Wilder et al., 2006) for understanding the relationship between buckling  
59 profiles and material parameters. Recent advances on buckling of thin films on a bi-layer compliant  
60 substrate of finite thickness can be found in Wang et al. (2020) and references cited therein.  
61 However, most of the existing mechanical models assume plane-strain deformation hypothesis,  
62 which is not always adequate, especially in case of narrow thin films on compliant substrates, as it  
63 has been recently pointed out by Jiang et al. (2008) by determining an analytical solution for the  
64 buckling of an Euler-Bernoulli beam on three-dimensional half-space and comparing analytical  
65 results with experimental data.

66 It is worth noting that most of the contributions dedicated to buckling of beams on elastic  
67 substrates, both regarding civil or mechanical/electronic engineering, assume the hypothesis of  
68 beams with infinite length; however, in some cases, with particular reference to shallow foundations  
69 in civil engineering, the beam length is finite and at least one order of magnitude larger than beam  
70 width; furthermore, the structural relationship between the foundation beam and the superstructure  
71 may need to be taken into consideration by adopting appropriate boundary conditions at beam ends.

72 Focusing on the buckling of beams with finite length, in Timoshenko and Gere (1961) a simply  
73 supported beam on Winkler soil was studied. Other boundary conditions, such as beam with fixed  
74 ends and beam with free ends, were studied and compared with the former (Hetenyi, 1946). In the  
75 context of sandwich plates, even if still modelled as beams on Winkler support, the finite length of  
76 the beam allowed Goodier and Hsu (1954) to highlight the presence of nonsinusoidal buckling

77 modes with displacements localized at the beam ends. Similar local buckling modes have been  
78 recently found by Tullini et al. (2013a) with a beam having free and pinned ends on a two-  
79 dimensional elastic medium; furthermore, the corresponding critical loads led to critical stresses  
80 lower than that typically assumed for sandwich panel design and derived from Reissner solution.  
81 Euler-Bernoulli beams resting on an elastic half-plane were also investigated by Gallagher (1974)  
82 by using a Chebyshev series expansion for representing the beam deflection.

83 In the present work, the buckling of Euler-Bernoulli beams with finite length resting in bilateral  
84 frictionless contact with an elastic three-dimensional half-space is studied by extending to this field  
85 of analysis the finite element-boundary integral equation (FE-BIE) coupling method introduced in  
86 Tullini and Tralli (2010) for the static analysis of foundation beams with varying boundary  
87 conditions. This method has already proven its effectiveness by comparing numerical results of  
88 static analyses with existing analytical solutions and other numerical results. In particular, the  
89 computational effort required by proposed method turned out to be significantly smaller than that of  
90 a standard Finite Element Model (FEM).

91 The FE-BIE coupling method has been originally introduced for the static analysis of both Euler-  
92 Bernoulli and Timoshenko beams in frictionless contact with a two-dimensional half-space (Tullini  
93 and Tralli, 2010) and it has been already extended to the corresponding buckling problem (Tullini et  
94 al., 2013a, Tullini et al., 2013b, Baraldi, 2019), and to the case of a fully adhesive contact (Tullini et  
95 al., 2012; Tezzon et al. 2015; Tezzon et al. 2016; Tezzon et al. 2018). Effects of sharp and smooth  
96 beam edges in the buckling of a Timoshenko beam in frictionless and bilateral contact with an  
97 elastic half-plane was analysed in Falope et al. (2020).

98 Here, attention is given to Euler-Bernoulli beams resting on a three-dimensional transversely  
99 isotropic elastic half-space, having the plane of isotropy parallel to the half-space boundary. The  
100 beam instability in horizontal direction, which may take place with beams having large length-to-  
101 width ratio (Kerr, 1974; Kerr, 1978), here is neglected and only vertical displacements are taken  
102 into account. Beam deflections are assumed to vary only along longitudinal direction, hence

103 uniform displacements along beam transversal direction are assumed. The proposed mixed  
104 variational formulation assumes as independent fields both the surface tractions and the beam  
105 displacements, whereas traditional variational formulations for beams and plates on half-space  
106 assume displacements as unknowns of the problem. The numerical model adopts Hermitian shape  
107 functions for the beam and piecewise constant function for the surface tractions. A set of numerical  
108 tests is performed for evaluating the effectiveness of the model in determining beam buckling loads  
109 and the corresponding modal shapes by varying the mechanical parameters characterizing the beam-  
110 substrate system and by considering the effect of beam length-to-width ratio. Several boundary  
111 conditions at beam ends are also taken into consideration. Numerical results are compared with  
112 existing analytical solutions, which are almost always dedicated to beams with infinite length, with  
113 particular attention to critical load values and to buckling wavelength.

## 114 **2. BASIC RELATIONSHIPS**

### 115 **2.1. Variational formulation**

116 This work considers a slender elastic beam with length  $L$  resting in bilateral and frictionless  
117 contact with a transversely isotropic half-space. The beam is referred to a Cartesian coordinate  
118 system  $(O; x, y, z)$ , where the  $x$ - $y$  plane defines the half-space boundary,  $x$  is assumed to be  
119 coincident with the centroidal axis of the beam,  $z$  is chosen in the downward transverse direction  
120 and it is normal to the plane of isotropy of the half-space. The beam has a symmetric cross-section  
121 shape with respect to the axis  $z$ , with height  $h$  and width  $b$  representing the overall cross-section  
122 dimensions in  $z$  and  $y$  direction, respectively. Moreover, a flat cross-section base is considered, in  
123 order to define a rectangular contact area between the beam and the half-space with constant width  
124  $b$  and length  $L$ , allowing to introduce the dimensionless parameter  $\chi = L/b$ . The beam is loaded at its  
125 ends by a concentrated compressive force  $P$  as shown in Fig. 1, where the simple case of beam  
126 rectangular cross-section is considered. A vertical load  $p(x)$  distributed along the beam axis can also  
127 be applied to the beam. Following the assumptions already adopted for the beam on isotropic half-

128 space subjected to static loads (Baraldi and Tullini, 2018), the beam experiences flexure only in  $x$ - $z$   
 129 plane, hence, together with the frictionless and bilateral conditions assumed between beam and  
 130 substrate, only a vertical half-space traction  $r(x, y)$  is acting upon the beam. The hypothesis of  
 131 frictionless contact allows a possible slip along the  $x$ - $y$  plane between the beam and the elastic  
 132 support.

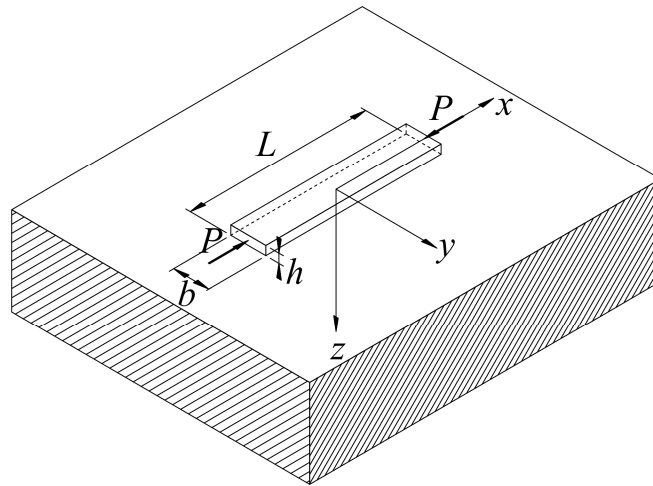
133 Focusing first on half-space behaviour, the three-dimensional problem for a homogeneous, linear  
 134 elastic and transversely isotropic half-space loaded by a point force normal to its boundary plane  
 135 has been studied by many authors, see (Michell, 1900; Liao and Wang, 1998; Kachanov et al.,  
 136 2003; Ding et al., 2006; Anyaegbunam, 2014; Marmo et al., 2017; Argatov and Mishuris, 2018;  
 137 Popov et al. 2019) and references cited therein. In particular, the vertical displacement  $w$  of a point  
 138 on the half-space boundary due to a generic normal traction  $r(x, y)$  is given by

$$139 \quad w(x, y, 0) = \frac{1}{\pi E_s} \int_{-b/2}^{b/2} \int_L \frac{r(\hat{x}, \hat{y}) d\hat{x} d\hat{y}}{d(x, y; \hat{x}, \hat{y})} \quad (1)$$

140 where

$$141 \quad d(x, y; \hat{x}, \hat{y}) = \sqrt{(x - \hat{x})^2 + (y - \hat{y})^2} \quad (2)$$

142



143

144

Fig. 1. Compressed beam resting on a half-space.

145 is the distance between the points  $(x, y, 0)$  and  $(\hat{x}, \hat{y}, 0)$ , and  $E_s$  is the equivalent elastic modulus of  
 146 the half-space along the vertical direction  $z$ . Details on such modulus can be found in the recent  
 147 contribution by Baraldi and Tullini (2020) and in references cited therein. However, for an isotropic  
 148 substrate, the equivalent elastic modulus  $E_s$  reduces to  $E_{\text{soil}}/(1-\nu_{\text{soil}}^2)$ , where  $E_{\text{soil}}$  and  $\nu_{\text{soil}}$  are Young  
 149 modulus and Poisson ratio of the isotropic substrate; correspondingly, Eq. (1) reduces to Boussinesq  
 150 solution (Kachanov et al., 2003; Johnson, 1985).

151 Following the considerations done in Baraldi and Tullini (2018), due to the theorem of work and  
 152 energy for exterior domains (Gurtin and Sternberg, 1961) and accounting for Eq. (1), the total  
 153 potential energy of the half-space is

$$154 \quad \Pi_s = -\frac{1}{2\pi E_s} \int_{-b/2}^{b/2} \int_L r(x, y) dx dy \int_{-b/2}^{b/2} \int_L \frac{r(\hat{x}, \hat{y}) d\hat{x} d\hat{y}}{d(x, y; \hat{x}, \hat{y})} \quad (3)$$

155 Focusing on beam behaviour, an Euler-Bernoulli beam model is assumed, and restricting the  
 156 analysis in the  $x$ - $z$  plane, beam vertical displacement can be written as  $w(x, y, z) = w(x)$ . The total  
 157 potential energy of the beam, including second order effects, can be written as

$$158 \quad \Pi_b = \frac{1}{2} \int_L [D_b (w''(x))^2 - P(w'(x))^2] dx - \int_L [(p(x) - \int_{-b/2}^{b/2} r(x, y) dy) w(x)] dx, \quad (4)$$

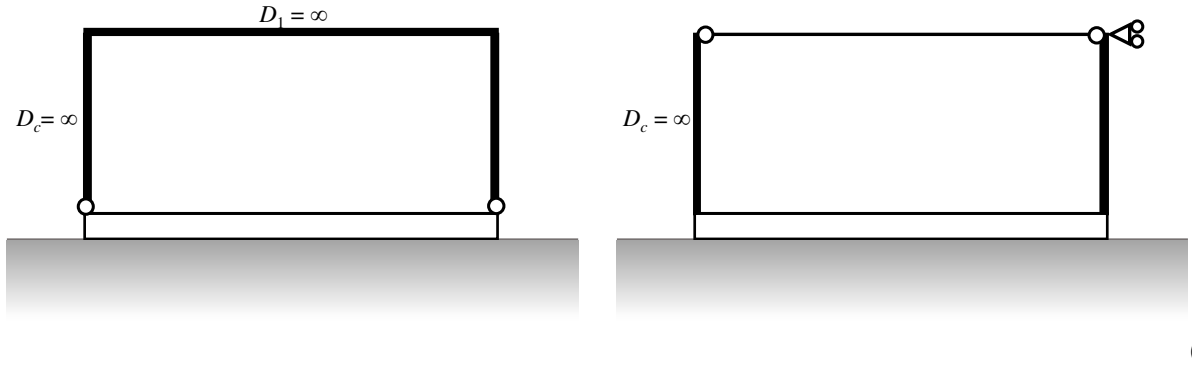
159 where prime denotes differentiation with respect to  $x$  and  $D_b = E_b J_b$ , with  $E_b$  being longitudinal  
 160 elastic modulus and  $J_b$  the second area moment of beam cross-section with respect to the  $y$  axis.

161 It is worth noting that Boussinesq solution (1) holds for a half-space loaded by surface tractions  
 162 normal to its boundary, which must be free to deform elsewhere. Consequently, external constraints  
 163 can not be applied to the substrate and the only constraints allowed are those imposed by the  
 164 superstructure to the foundation beam. Thus, only constraint equations  $R_i(w, w') = 0$  between  
 165 displacements or rotations may be assigned along the beam axis. For example, a pinned-pinned  
 166 beam requires the equation  $R_1 = w(L/2) - w(-L/2) = 0$ , which may refer to a rigid frame, whose  
 167 beam and columns have flexural rigidity  $D_c = \infty$  and  $D_1 = \infty$ , respectively, and the columns are  
 168 hinged to the foundation beam (Fig. 2a); thus, the structure enforces zero relative displacement at

169 the beam ends, but allows independent rotations. Likewise, a beam with sliding ends requires the  
 170 following system of equations  $R_1 = w'(L/2) - w'(-L/2) = 0$  and  $R_2 = w'(L/2) + w'(-L/2) = 0$ , which  
 171 may refer to a frame with rigid columns ( $D_c = \infty$ ) and simply supported beam with infinite axial  
 172 stiffness and fixed horizontal displacements; thus, the structure prevents rotations at the ends of the  
 173 foundation beam but allows independent vertical displacements (Fig. 2b). It is worth noting that the  
 174 term ‘sliding’ is here adopted for defining a specific restraint condition for the displacements and  
 175 rotations at the beam ends and it is not to be confused with the potential slip that can occur between  
 176 the beam and the elastic support allowed by the frictionless contact. The constraint equations can be  
 177 included in the total potential energy  $\Pi$  of the beam-substrate system by means of a penalty  
 178 approach. Hence, making use of Eqs. (3) and (4), the total potential energy of the beam-substrate  
 179 system turns out to be (Reddy, 2006):

$$180 \quad \Pi(w, r) = \Pi_b(w, r) + \Pi_s(r) + \frac{k}{2} \sum_i [R_i(w, w')]^2, \quad (5)$$

181 where  $k$  is the penalty parameter, whose value should be large enough to satisfy the constraint  
 182 equations accurately.



184 Fig. 2. Beam with pinned ends on a half-space, given by a rigid frame with columns hinged to the  
 185 foundation beam (a); beam with sliding ends on a half-space, given by a frame with rigid columns  
 186 and simply supported beam (b).

187 Variational formulation analogous to Eq. (5) was obtained in (Kikuchi, 1980; Kikuchi and Oden,  
 188 1988; Bielak and Stephan, 1983) for beams resting on a Pasternak soil, in (Tullini and Tralli, 2010;



189 Baraldi and Tullini, 2017) for beams and frames resting in bilateral frictionless contact with an  
190 elastic half-plane and in Baraldi and Tullini (2018) for a Timoshenko beam in bilateral frictionless  
191 contact with an elastic isotropic half-space. Moreover, mixed variational principle similar to Eq. (5)  
192 was used in Tullini et al. (2012) to study axially loaded thin structures perfectly bonded to an elastic  
193 substrate and in (Tullini et al., 2013a; Tullini et al., 2013b; Baraldi, 2019) to determine the buckling  
194 loads of beams in frictionless contact with an elastic half-plane and an elastic layer in plane state.  
195 Beams in perfect adhesion with an elastic half-plane are considered in (Tezzon et al., 2015; Tezzon  
196 et al., 2016). Differently with respect the proposed approach, traditional variational formulations are  
197 defined in terms of foundation displacements only (Selvadurai, 1979b; Selvadurai, 1980;  
198 Selvadurai, 1984).

199 Following the considerations already done in Baraldi and Tullini (2018), it must be pointed out  
200 that the beam model hypothesis implies vertical displacement  $w$  varying only along  $x$  direction and  
201 uniform vertical displacement along beam width. This hypothesis is satisfied if the beam cross-  
202 section is infinitely rigid with respect to the half-space in the  $y$  direction, then the distribution of  
203 contact tractions  $r$  in such direction is expected to be equal to the one generated by a rigid indenter  
204 with width  $b$  in a plane strain problem (Johnson, 1985; Kachanov et al. 2003) and characterized by  
205 singularities close to section ends. However, uniform tractions  $r$  along beam width are often taken  
206 into consideration when analytic solutions of infinite beams on elastic half-space are searched  
207 (Jiang et al., 2008, Tarasovs and Andersons, 2008), and the consequent non-uniform beam  
208 displacement along transversal direction is simplified by considering the displacement at beam  
209 centerline or an average value of transversal deflection. The two different approaches were  
210 investigated analytically for first by Biot (1937) for the static analysis of infinite beams and by  
211 Murthy (1973) for the corresponding stability analysis.

212

213 **2.2 Discrete model**

214 A simple discretization of the beam-substrate system can be created by subdividing the beam  
 215 into FEs of equal length  $l_{xi} = L/n_x$ , where  $n_x$  is the number of subdivisions in  $x$  direction. The contact  
 216 surface underneath the beam may be divided in  $x$  direction with the same number of subdivisions  
 217 assumed for the beam, whereas in  $y$  direction, i.e. across the beam width, the number of  
 218 subdivisions  $n_y$  can be assumed larger than one in order to correctly modelling the non-uniform  
 219 pressures generated by uniform displacements. In particular, for correctly describing reactions at  
 220 contact surface edges with a small number of surface subdivisions, it is common to use power  
 221 graded meshes (Erwin and Stephan, 1992; Graham and McLean, 2006), which are characterized by  
 222 a grading exponent  $\beta \geq 1$  that allows to obtain small subdivisions close to surface edges. The same  
 223 type of power graded discretization can be also adopted in  $x$  direction close to beam ends, in order  
 224 to obtain small subdivisions at the corners of the foundation. However, the convergence tests  
 225 already done by authors with the static case (Tullini et al., 2013a) showed that this type of mesh  
 226 refinement does not influence significantly the accuracy of numerical results, hence, it will not be  
 227 adopted in this work. Then, a piecewise constant discretization of contact surface tractions is  
 228 adopted by assuming constant shape functions, whereas classical Hermitian polynomials are  
 229 assumed as beam shape functions (Reddy, 2006).

230 The stationarity condition of the total potential energy  $\Pi(w, r)$  written in discrete form provides  
 231 the following system:

$$232 \begin{bmatrix} \frac{D_b}{L^3} \left( \tilde{\mathbf{K}}_b - \frac{PL^2}{D_b} \tilde{\mathbf{K}}_g \right) & b \tilde{\mathbf{H}} \\ b \tilde{\mathbf{H}}^T & -\frac{b}{E_s} \tilde{\mathbf{G}} \end{bmatrix} \begin{Bmatrix} \mathbf{q} \\ \mathbf{r} \end{Bmatrix} = \begin{Bmatrix} \mathbf{F} \\ \mathbf{0} \end{Bmatrix}, \quad (6)$$

233 where the vector  $\mathbf{q}$  collects beam nodal displacements,  $\mathbf{r}$  denotes the vector of the constant soil  
 234 reactions,  $\mathbf{F}$  is the vector of the external loads,  $D_b/L^3 \tilde{\mathbf{K}}_b$  is the elastic stiffness matrix of the beam,  
 235  $P/L \tilde{\mathbf{K}}_g$  is the geometric (or incremental) stiffness matrix (Reddy, 2006; Tullini et al., 2013a), and

236 the elements of the matrices  $\tilde{\mathbf{H}}$  and  $\tilde{\mathbf{G}}$  are reported in Baraldi and Tullini (2018). Details of penalty  
 237 approaches adopted for modifying beam stiffness matrix  $\tilde{\mathbf{K}}_b$  are reported in Appendix. The system  
 238 in Eq. (6) yields the following solution

$$239 \quad \mathbf{r} = E_s \tilde{\mathbf{G}}^{-1} \tilde{\mathbf{H}}^T \mathbf{q}, \quad (7)$$

$$240 \quad [\tilde{\mathbf{K}}_b - \lambda \tilde{\mathbf{K}}_g + (\alpha L)^3 \tilde{\mathbf{K}}_{\text{soil}}] \mathbf{q} = \frac{L^3}{D_b} \mathbf{F}, \quad (8)$$

241 where  $\tilde{\mathbf{K}}_{\text{soil}}$  is the stiffness matrix of the soil or three-dimensional half-space

$$242 \quad \tilde{\mathbf{K}}_{\text{soil}} = \tilde{\mathbf{H}} \tilde{\mathbf{G}}^{-1} \tilde{\mathbf{H}}^T, \quad (9)$$

243 the axial load multiplier is  $\lambda = PL^2/D_b$ , and  $\alpha L$  is the well-known (Biot, 1937; Vesic, 1961;  
 244 Selvadurai, 1979a; Baraldi and Tullini, 2018) parameter characterizing the soil-foundation system:

$$245 \quad \alpha L = \sqrt[3]{\frac{E_s b L^3}{D_b}}. \quad (10)$$

246 The adopted mixed finite element is particularly simple and effective, as shown in Baraldi and  
 247 Tullini (2018) for the static case, where the numerical properties of the proposed FE model are also  
 248 discussed. With regard to the determination of critical load  $P_{\text{cr}}$ , a homogeneous system associated to  
 249 Eq. (8) must be considered and the buckling loads are given by the roots  $\lambda_{\text{cr}}$  of the equation  
 250  $\det[\tilde{\mathbf{K}}_b - \lambda \tilde{\mathbf{K}}_g + (\alpha L)^3 \tilde{\mathbf{K}}_{\text{soil}}] = 0$ , which can be suitably reduced to a standard eigenvalue problem.

251 Introducing the definition of Euler critical load:

$$252 \quad P_{\text{cr,E}} = \frac{\pi^2 D_b}{L^2}, \quad (11)$$

253 the dimensionless buckling loads turn out to be given by  $P_{\text{cr}}/P_{\text{cr,E}} = \lambda_{\text{cr}}/\pi^2$ .

### 254 3. NUMERICAL TESTS

255 The buckling of Euler-Bernoulli beams with finite length is investigated by assuming three  
 256 different boundary conditions at beam ends, following the same approach adopted for the beam on

257 elastic half-plane (Tullini et al., 2013a). However, a preliminary convergence test is performed by  
258 determining the first three critical loads of a beam with free ends assuming two  $\alpha L$  and  $\chi$  values, for  
259 increasing beam subdivisions and by considering several contact surface discretization types along  
260 beam width. Then, assuming a beam with aspect ratio  $\chi = 10$ , critical loads and modal shapes are  
261 determined for increasing  $\alpha L$ . Finally, several considerations are done varying parameter  $\chi$ .

262

### 263 3.1. Convergence test

264 The first three critical loads of a compressed beam with free ends on half-space are determined  
265 by considering four different geometrical and mechanical conditions represented by the parameters  
266  $\alpha L$  equal to 5 and 25 and  $\chi$  equal to 10 and 100. Numerical reference solutions  $P_{cr,f,i}^{ref}$ , with  $i = 1, 2,$   
267 3, are determined by assuming  $n_x = 2^{11}$  and a  $n_y = 7$  with a power-graded discretization with  $\beta = 3$   
268 (Tab. 1); then, the influence of the approximation of contact tractions along beam width is evaluated  
269 by considering the simple case with  $n_y = 1$ , namely a constant traction along beam width, and the  
270 more accurate case with a power-graded subdivision with  $n_y = 3$  and  $\beta = 3$ . Fig. 3 shows the relative  
271 differences  $\delta P_{cr,f,i} = (P_{cr,f,i}^{ref} - P_{cr,f,i}) / P_{cr,f,i}^{ref}$  obtained with the two proposed discretization types for  
272 increasing  $n_x$ . Differences turn out to have the same behaviour of those determined for the static  
273 case in terms of maximum vertical displacement and contact traction, since they tend to nonzero  
274 values instead of tending to zero. In general, the critical loads obtained with  $n_y = 3$  are quite close to  
275 reference solutions and differences generally tend to be less than 1% for  $n_x > 2^7$  with  $\alpha L = 5$  and  $n_x$   
276  $> 2^8$  with  $\alpha L = 25$ ; in particular, with  $\alpha L = 25$ , differences obtained for 1<sup>st</sup> and 2<sup>nd</sup> critical loads,  
277 which are coincident, start to converge for  $n_x > 2^7$ , with values close to 0.4% with  $\chi = 10$  and 0.2%  
278 with  $\chi = 100$ , highlighting that long beams on stiff half-space are less influenced by the subdivision  
279 refinement along  $x$  direction. The critical loads obtained with  $n_y = 1$  turn out to be less accurate with  
280 respect to reference solutions and differences are never less than 1% in the four cases considered.  
281 Convergence tests show that  $\alpha L$  parameter slightly influence the accuracy of the results, with a

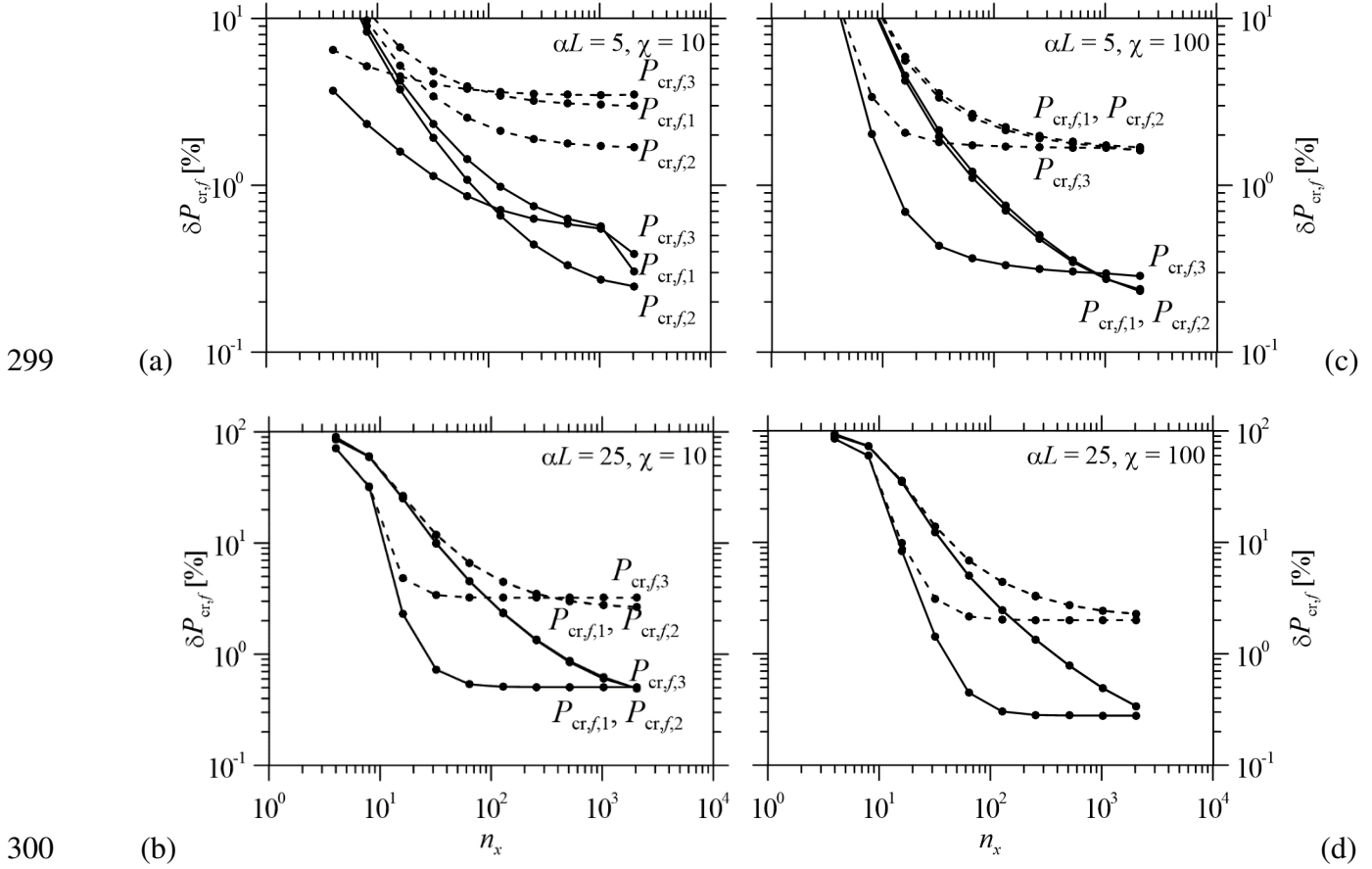
282 better convergence obtained with  $\alpha L = 25$ , whereas the differences obtained with  $\chi = 100$  are  
 283 slightly smaller than those obtained with  $\chi = 10$ , highlighting the necessity of a more accurate  
 284 contact surface discretization in case of a short beam or a beam with a small length-to-width ratio.  
 285 However, the order of magnitude of differences obtained with  $n_y = 1$  is still acceptable for  
 286 performing the upcoming numerical tests, since differences are generally less than 5% with  $n_x > 2^7$ .  
 287 In the following numerical test, the buckling loads are determined by assuming  $n_x = 2^7$  and  $n_y = 3$   
 288 with a power-graded discretization with  $\beta = 3$ .

289 It is worth noting that the critical loads determined by assuming constant tractions along beam  
 290 width turn out to be smaller than those obtained both with a less and more accurate contact surface  
 291 discretization along beam width. This aspect is in agreement with the results obtained by Murthy  
 292 (1973) for the stability of beams with infinite length, since critical loads obtained with uniform  
 293 reactions across beam width and assuming beam deflections along its longitudinal axis turned out to  
 294 be smaller than critical loads obtained with a reaction profile across beam width same as that of a  
 295 rigid stamp.

$P_{cr,f,i}^{ref} / [P_{cr,E}(\alpha L)^2]$	$\alpha L = 5$		$\alpha L = 25$	
	$\chi = 10$	$\chi = 100$	$\chi = 10$	$\chi = 100$
1	0.1312	0.3088	0.1040	0.1809
2	0.1731	0.3262	0.1040	0.1809
3	0.4050	0.6785	0.1641	0.3130

296 Tab. 1. Reference critical loads for a compressed beam with free ends on elastic half-space,  
 297 obtained with  $n_x = 2^{11}$  and a power-graded subdivision along y direction with  $n_y = 7$  and  $\beta = 3$ .

298



299 (a) (c)

300 (b) (d)

301 Fig. 3. Relative differences for the first three critical loads versus the overall number of

302 subdivisions along beam length for a compressed beam with free ends with  $\alpha L = 5$  (a, c) and 25 (b,

303 d), with  $\chi = 10$  (a, b) and  $\chi = 100$  (c, d). Results obtained with  $n_y = 1$  (dashed lines) and  $n_y = 3$

304 (continuous lines), assuming results in Tab. 1 as reference.

### 306 3.2. Beam of finite length with sliding ends

307 The buckling of a beam with sliding ends on elastic half-space, with  $\chi = 10$ , is considered (Fig.

308 2b). The constraint equations to be used in Eq. (5) are  $R_1 = w'(L/2) - w'(-L/2) = 0$  and  $R_2 = w'(L/2)$

309  $+ w'(-L/2) = 0$ . Details of stiffness matrices of the elements at beam ends, together with  $\tilde{\mathbf{K}}_b$  for the

310 entire beam are reported in Appendix. Assuming a penalty parameter  $k = 10^9 l_i D_b/L^3$  that ensures a

311 stable numerical solution of Eq. (8), Fig. 4a shows dimensionless critical loads  $P_{cr,s}/P_{cr,E}$  varying

312 with  $\alpha L$ . The numerical results show a behaviour analogous to the same beam type on an elastic

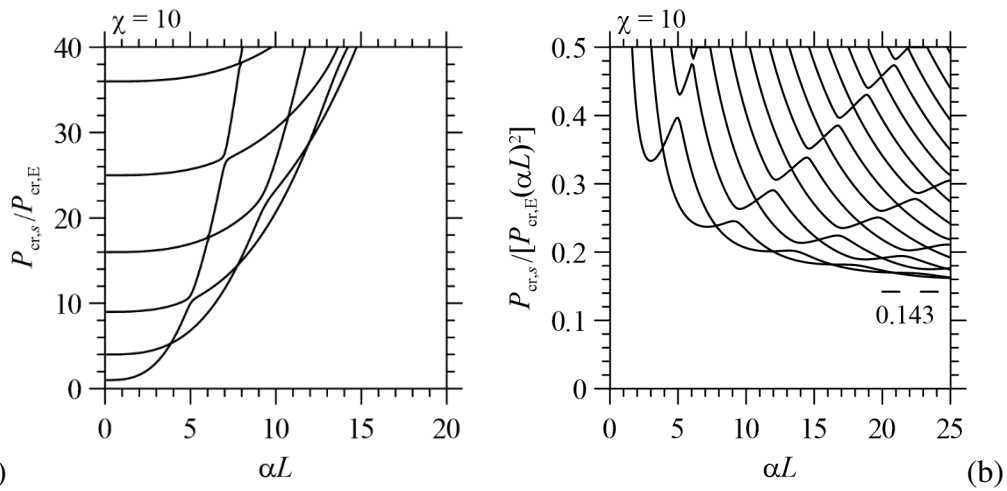
313 half-plane, since critical loads increase for increasing  $\alpha L$  and present crossing points and curve

314 veering. It is worth noting that, for  $\alpha L$  equal to zero, critical loads are equal to the values  
 315  $P_{cr,m(0)}/P_{cr,E} = m^2$ , with  $m = 1, 2, 3, \dots$ , typical of a beam with pinned or sliding ends without a  
 316 supporting medium. Fig. 4b shows the ratio  $P_{cr,s}/[P_{cr,E}(\alpha L)^2]$  versus the parameter  $\alpha L$ . For  
 317 increasing  $\alpha L$ , the ratios corresponding to the first eigenvalue do not converge to a stable value,  
 318 whereas in case of a beam on elastic half-plane such convergence was evident and the  
 319 corresponding critical load was equal to that of a beam with infinite length (Tullini et al., 2013a).  
 320 However, for  $\alpha L$  equal to 50, the first two critical loads are close to

$$321 \quad P_{cr,s,1} = P_{cr,s,2} = 0.143 P_{cr,E}(\alpha L)^2. \quad (12)$$

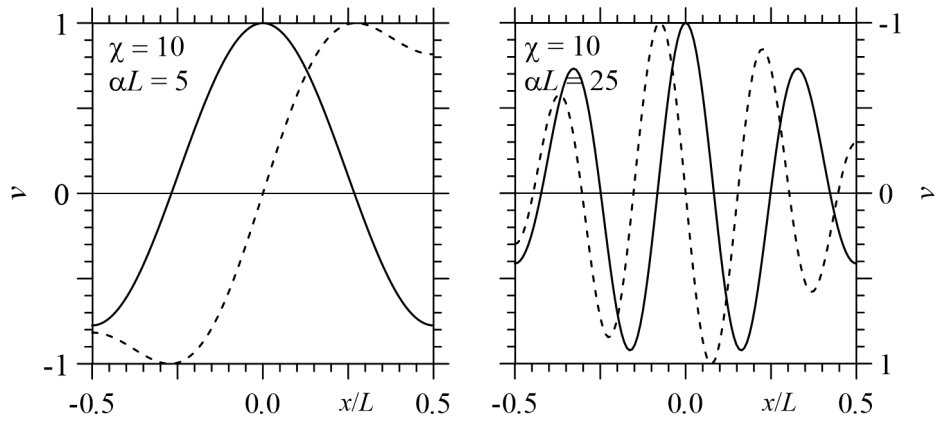
322 This result will be further investigated in the final part of the manuscript by evaluating the influence  
 323 of  $\chi$  on critical load values and by evaluating their relationship with respect to the critical loads of a  
 324 beam on elastic half-plane.

325 Fig. 5 shows first and second mode shapes of the beam with sliding ends for two  $\alpha L$  values.  
 326 Mode shapes are analogous to those of a beam with sliding ends on elastic half-plane, since they are  
 327 sinusoidal and characterized by an increasing number of half-waves for increasing  $\alpha L$ .



328 (a) (b)

329 Fig. 4. Dimensionless critical loads  $P_{cr,s}$  versus  $\alpha L$  for a beam with sliding ends on elastic half-  
 330 space.



331

(a)

(b)

332

Fig. 5. First (continuous line) and second (dashed line) mode shapes for a beam with sliding ends

333

and  $\alpha L$  equal to 5 (a) and 25 (b).

334

### 335 3.3. Beam of finite length with pinned ends

336

The buckling of a beam with pinned ends on elastic half-space is considered (Fig. 2a). The

337

constraint equation to be applied to Eq. (5) is  $R_1 = w(L/2) - w(-L/2) = 0$ , details for obtaining the

338

stiffness matrix of the beam are given in Appendix. Assuming a penalty parameter  $k = 10^6 D_b/L^3$ ,

339

Fig. 6a shows dimensionless critical loads  $P_{cr,p}/P_{cr,E}$  are versus  $\alpha L$ . For  $\alpha L$  equal to zero, critical

340

loads converge to the values already highlighted in the previous subsection  $P_{cr,m}(0)/P_{cr,E} = m^2$ , with

341

$m = 1, 2, 3, \dots$ , typical of a beam with pinned ends without any other support. Critical loads increase

342

for increasing  $\alpha L$  and present crossing points and curve veering, however the first critical load

343

appears to be quite far from other results, whereas second critical load is quite close to the third and

344

fourth ones, differently with respect to the beam with pinned ends on elastic half-plane.



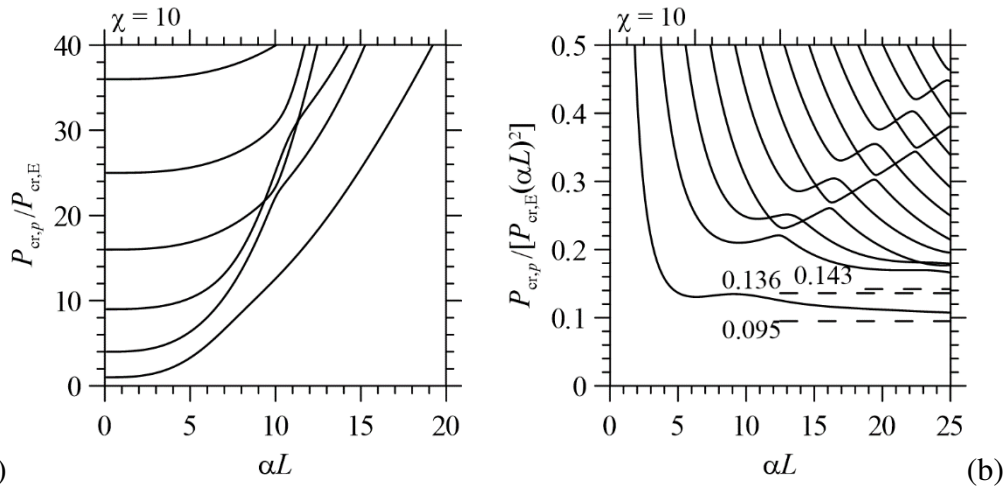


Fig. 6. Dimensionless critical loads  $P_{cr,p}$  versus  $\alpha L$  for a beam with pinned ends on half-space.

Considering Fig. 6b showing the ratio  $P_{cr,p}/[P_{cr,E}(\alpha L)^2]$  versus the parameter  $\alpha L$ , numerical results do not show a convergence to stable values, however, for  $\alpha L$  equal to 50, the first critical load is equal to:

$$P_{cr,p,1} = 0.095 P_{cr,E}(\alpha L)^2, \quad (13)$$

whereas the second critical load is equal to:

$$P_{cr,p,2} = 0.136 P_{cr,E}(\alpha L)^2, \quad (14)$$

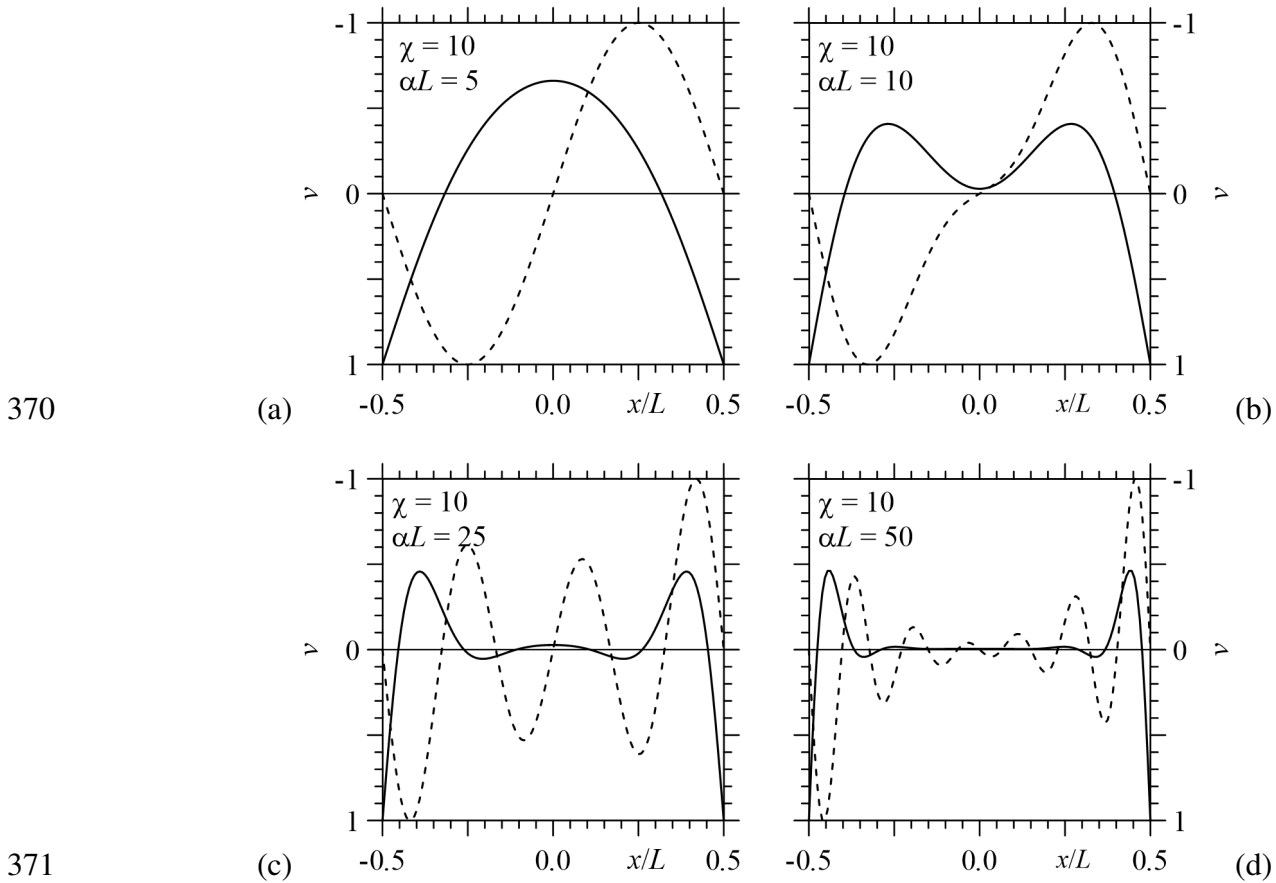
which is slightly smaller but quite close to Eq. (12). Such a value is reached by the third and fourth critical loads for increasing  $\alpha L$ :

$$P_{cr,p,3} = P_{cr,p,4} = 0.143 P_{cr,E}(\alpha L)^2. \quad (15)$$

Furthermore,  $P_{cr,p,2}$  is 95% of  $P_{cr,s,1}$ , this ratio is larger than the corresponding one obtained for the beam on elastic half-plane, which is  $0.106 / 0.121 = 88\%$  (Tullini et al., 2013a).

Fig. 7 shows first and second mode shapes for several  $\alpha L$  values. For  $\alpha L = 5$  (Fig. 7a), first and second mode shapes are sinusoidal, whereas for  $\alpha L = 10$  (Fig. 7b), first and second mode shapes can not be described by sinusoidal functions, similarly to the case of a beam with pinned ends on elastic half-plane. For  $\alpha L = 25$  (Fig. 7c), the first mode shape is characterized by large deflections at beam ends, but the second mode shape is sinusoidal. Increasing  $\alpha L$  (Fig. 7d), the first mode shape has the

364 same behaviour found for the beam with pinned ends on elastic half-plane, characterized by large  
 365 deflections at beam ends and negligible displacements near beam midpoint, whereas the second  
 366 mode shape is characterized by large deflections at beam ends and sinusoidal deflections not  
 367 negligible along its length. This behaviour may justify the corresponding critical load (Eq. 14),  
 368 which is quite close to the third and fourth critical loads and to Eq. (12), which are typical of  
 369 sinusoidal mode shapes.



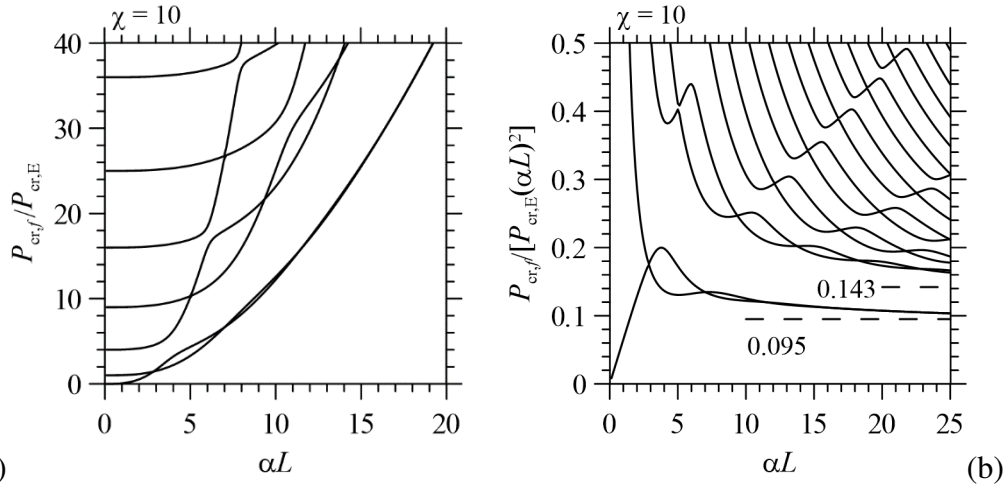
372 Fig. 7. First (continuous line) and second (dashed line) mode shapes for a beam with pinned ends  
 373 on half-space and  $\alpha L$  equal to 5 (a), 10 (b), 25 (c) and 50 (d).

374

### 375 3.4. Beam of finite length with free ends

376 The buckling of a beam with free ends on elastic half-space is finally considered. In Fig. 8a, the  
 377 dimensionless critical loads  $P_{cr,f}/P_{cr,E}$  are plotted versus  $\alpha L$ , whereas Fig. 8b shows the ratio  
 378  $P_{cr,f}/[P_{cr,E}(\alpha L)^2]$  versus the parameter  $\alpha L$ . Critical loads increase for increasing  $\alpha L$  and present

379 crossing points and curve veering. First and second critical loads, which are separated with respect  
 380 to other results, present some crossing points and both converge to the value given in Eq. 13 for  $\alpha L$   
 381 = 50, whereas the third and fourth eigenvalues converge to Eq. 12.



382 (a) (b)  
 383 Fig. 8. Dimensionless critical loads  $P_{cr,f}$  versus  $\alpha L$  for a beam with free ends on half-space.

384  
 385 Fig. 9 shows first and second mode shapes for increasing  $\alpha L$ . Analogously to the case of the  
 386 beam with free ends on elastic half-plane, for  $\alpha L = 1$  (Fig. 9a) the first mode shape represents a  
 387 rigid body rotation and the corresponding critical load tends to zero, whereas the second mode  
 388 shape is sinusoidal. For  $\alpha L = 5$  (Fig. 9b), after the first intersection point between first and second  
 389 critical load curves, the first mode shape is sinusoidal, but the second one is antisymmetric and  
 390 characterized by large displacements at beam ends. Increasing  $\alpha L$  (Figs. 9c and 9d), both mode  
 391 shapes are characterized by large displacements at beam ends and negligible deformations close to  
 392 beam midpoint. The symmetric mode shapes presented in Figs. 9a-d turn out to be coincident with  
 393 the first mode shape obtained for the beam with pinned ends.

394

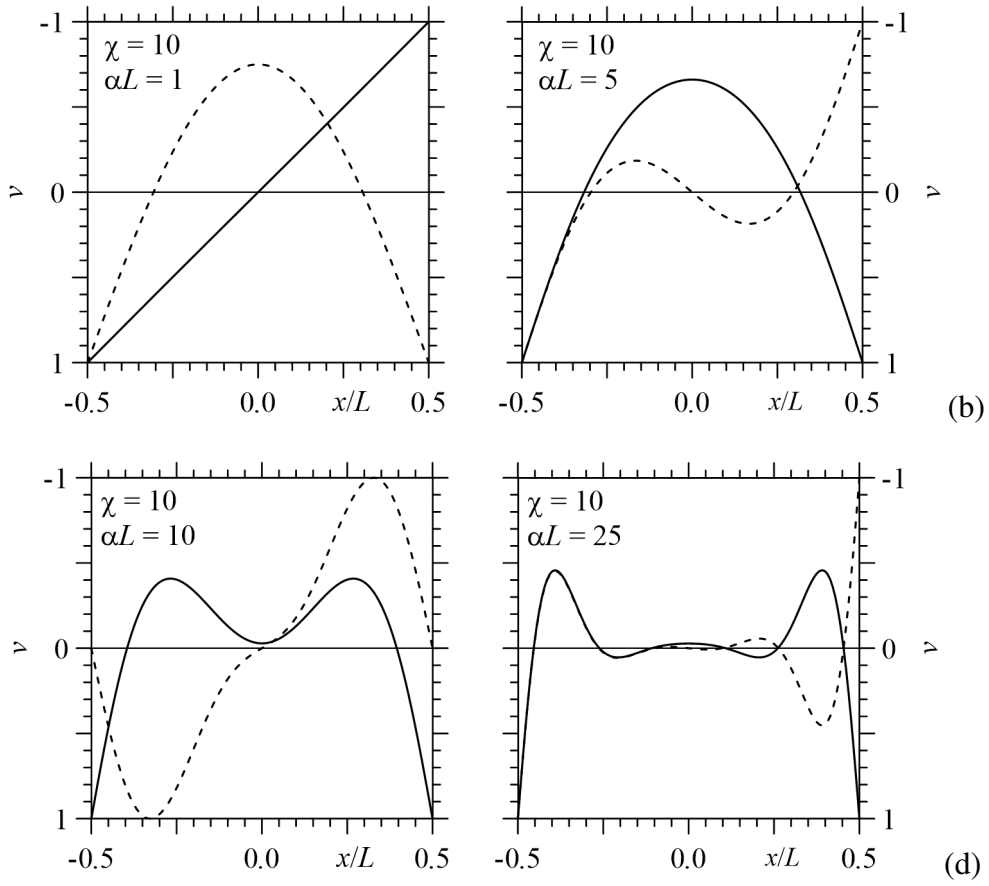


Fig. 9. First (continuous line) and second (dashed line) mode shapes for a beam with free ends and  $\alpha L$  equal to 1 (a), 5 (b), 10 (c) and 25 (d).

#### 4. INFLUENCE OF BEAM WIDTH ON OVERALL BEAM BUCKLING

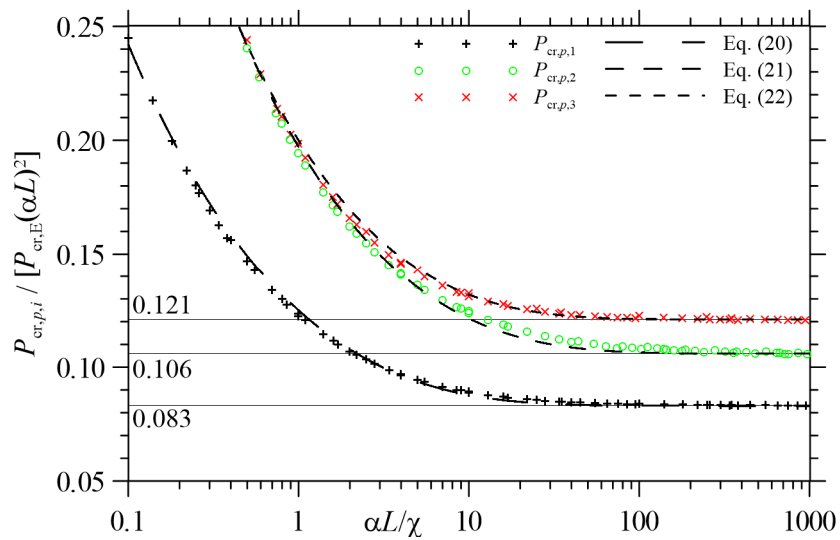
In the previous section it was observed that, for large  $\alpha L$  values, the first buckling load  $P_{cr,p,1}$  of the beam with pinned ends turns out to be coincident with the first and second critical loads of a beam with free ends, i.e.  $P_{cr,p,1} = P_{cr,f,1} = P_{cr,f,2}$ , whereas the third and fourth buckling loads  $P_{cr,f,3} = P_{cr,f,4}$ , and  $P_{cr,p,3} = P_{cr,p,4}$  are coincident with the first two buckling loads  $P_{cr,s,1} = P_{cr,s,2}$  of a beam with sliding ends. Nevertheless, the numerical tests performed in the previous section are characterized by beam length-to-width ratio  $\chi = 10$ , but the critical load values presented in Eqs. (12), (13) and (14), obtained with beams on a stiff soil having  $\alpha L = 50$ , strictly depend on  $\chi$ . Focusing on the behavior of a beam with pinned ends with  $\alpha L = 50$  and varying  $\chi$ , further values of  $P_{cr,p,1}$  ( $= P_{cr,f,1} = P_{cr,f,2}$ ),  $P_{cr,p,2}$ , and  $P_{cr,p,3}$  ( $= P_{cr,p,4} = P_{cr,f,3} = P_{cr,f,4} = P_{cr,s,1} = P_{cr,s,2}$ ) are collected in Tab.2.

410 Dimensionless critical loads increase for increasing  $\chi$ ; moreover, the second dimensionless  
 411 critical load tends to be more and more close to the third one increasing  $\chi$ . For example, for  $\chi = 1$   
 412 the ratio between  $P_{cr,p,2}$  and  $P_{cr,p,3}$  is close to 0.9, whereas for  $\chi = 100$  the same ratio is close to 0.98.  
 413 Fig. 10 shows the first three dimensionless critical loads of a beam on half-space, namely  $P_{cr,p,1}$   
 414 (plus symbols),  $P_{cr,p,2}$  (circles), and  $P_{cr,p,3}$  (crosses) for increasing  $\alpha L/\chi = ab$  by considering several  
 415  $\alpha L$  and  $\chi$  combinations.

	2D	$\chi = L/b$								
	Tullini et al., 2013a	0.1	1	2	3	4	5	10	50	100
$P_{cr,p,1}/[P_{cr,E}(\alpha L)^2]$	0.083	0.083	0.084	0.086	0.087	0.088	0.089	0.095	0.124	0.147
$P_{cr,p,2}/[P_{cr,E}(\alpha L)^2]$	0.106	0.107	0.112	0.115	0.119	0.122	0.125	0.136	0.194	0.240
$P_{cr,p,3}/[P_{cr,E}(\alpha L)^2]$	0.121	0.122	0.124	0.126	0.128	0.130	0.133	0.143	0.199	0.244

416 Tab. 2 – Dimensionless critical loads of a beam on half-space with  $\alpha L = 50$  varying  $\chi$ .

417



418

419 Fig. 10. First three dimensionless critical loads of a beam on half-space versus  $\alpha L/\chi$ .

420 It is worth noting that for small  $\chi$  values,  $\alpha L/\chi$  increases and the beam has a very short length  
421 with respect to its width. However, buckling modes along beam width are not allowed by the  
422 proposed model, since deformations along beam width are neglected; hence, the case of a beam  
423 having a large width with respect to its length numerically converges to a plane strain condition. In  
424 fact, for  $\chi$  tending to zero or  $\alpha b$  tending to infinite, dimensionless critical loads  $P_{cr,p,i}$  for  $i = 1, 2, 3$ ,  
425 turn out to converge to the corresponding ones obtained for the beam on elastic half-plane  
426 (continuous lines in Fig. 10) (Tullini et al., 2013a):

$$427 \quad P_{cr,p,1}^{2D} = 0.083 P_{cr,E} (\alpha L)^2, \quad (16)$$

$$428 \quad P_{cr,p,2}^{2D} = 0.106 P_{cr,E} (\alpha L)^2, \quad (17)$$

$$429 \quad P_{cr,p,3}^{2D} = P_{cr,s,1}^{2D} = 0.121 P_{cr,E} (\alpha L)^2 = 3/(2^{4/3} \pi^2) P_{cr,E} (\alpha L)^2. \quad (18)$$

430 Nonetheless, in the plane strain state, the parameter  $\alpha L$  contains the ratio  $E_b/(1-\nu_b^2)$ , where  $\nu_b$  is the  
431 Poisson ratio of the beam, instead of the beam modulus  $E_b$ , as in a plane stress state.

432 Eq. (18) allows evaluation of the critical strain in a form frequently used in the design of  
433 structural sandwich panels (Allen, 1969; Ley et al., 1999; Davies, 2001) and in flexible and  
434 stretchable electronics (Huang, 2005; Genzer and Groenewold, 2006; Jiang et al., 2008):

$$435 \quad e_{cr,s}^{2D} = \frac{P_{cr,s,1}^{2D}}{E_b b h} = 0.52 \left( \frac{E_s}{E_b} \right)^{2/3}. \quad (19)$$

436 In order to fit numerical results and obtaining approximated functions for the first three  
437 dimensionless critical loads of a beam on elastic half-space, the following expressions are proposed  
438 and added with dashed lines to Fig. 10:

$$439 \quad P_{cr,p,1} / [P_{cr,E} (\alpha L)^2] = 0.083 \coth[0.80 (\alpha b)^{0.35}], \quad (20)$$

$$440 \quad P_{cr,p,2} / [P_{cr,E} (\alpha L)^2] = 0.106 \coth[0.60 (\alpha b)^{0.35}], \quad (21)$$

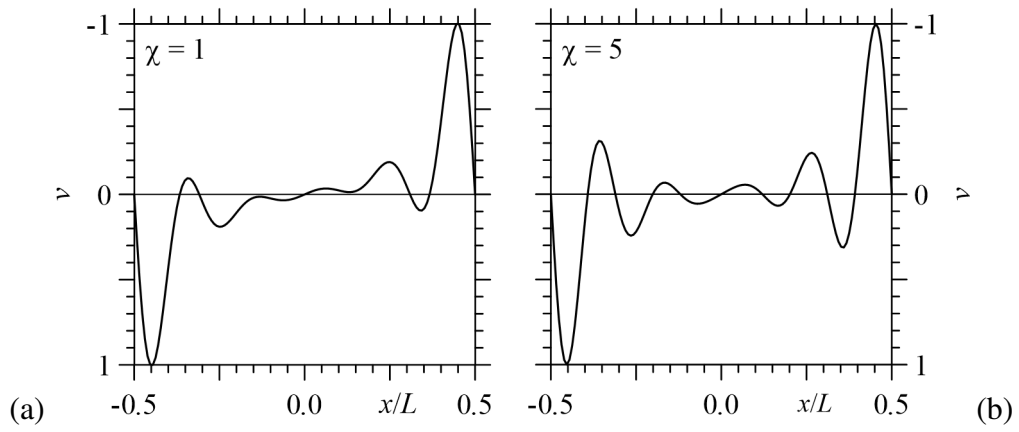
$$441 \quad P_{cr,p,3} / [P_{cr,E} (\alpha L)^2] = 0.121 \coth[0.70 (\alpha b)^{0.35}]. \quad (22)$$

442 For increasing  $ab$  the proposed approximated expressions converge to the numerical results of a  
443 beam on elastic half-plane and are characterized by determination factor  $R^2$  close to 1, in particular  
444 for all  $ab$  values with Eq. (22) and for  $ab < 10$  with Eqs. (20) and (21).

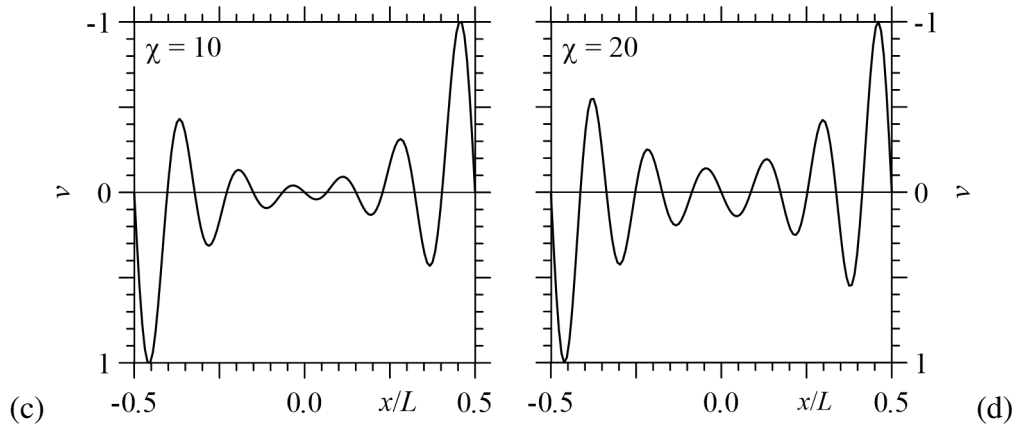
445 Numerical results in Fig. 10 also show that  $P_{cr,p,2}$  and  $P_{cr,p,3}$  turn out to be coincident for  
446 decreasing  $ab$  or increasing  $\chi$ . This aspect is justified by the mode shapes corresponding to  $P_{cr,p,2}$   
447 obtained with large  $\alpha L$  values, already shown with dashed lines in Figs. 7c and 7d, and  
448 characterized by sinusoidal deflections with large amplitude close to beam ends. Analogous  
449 sinusoidal displacements are shown in Fig. 11 for  $\alpha L = 50$  and increasing  $\chi$ , hence decreasing  $ab$ .  
450 Large beam deflections are located close to beam ends in all the cases considered, but beam  
451 displacements along beam length increase and tend to become sinusoidal for increasing  $\chi$ . In  
452 particular, Figs. 11e and 11f show that beam deflections are sinusoidal with different amplitude  
453 along beam length and wavelength appears to be uniform. These modal shapes are quite similar to  
454 those of a beam with sliding ends (Fig. 5b) and the corresponding wavelengths are investigated in  
455 the next sub-section.

456 It is worth noting that the buckling behaviour of a beam with pinned ends on half-space turns out  
457 to be quite similar to that of the same beam on Winkler substrate (Hetenyi, 1946), which is  
458 characterized by the second critical load converging to the same value of the third and fourth ones,  
459 with a sinusoidal modal shape over the entire beam length.

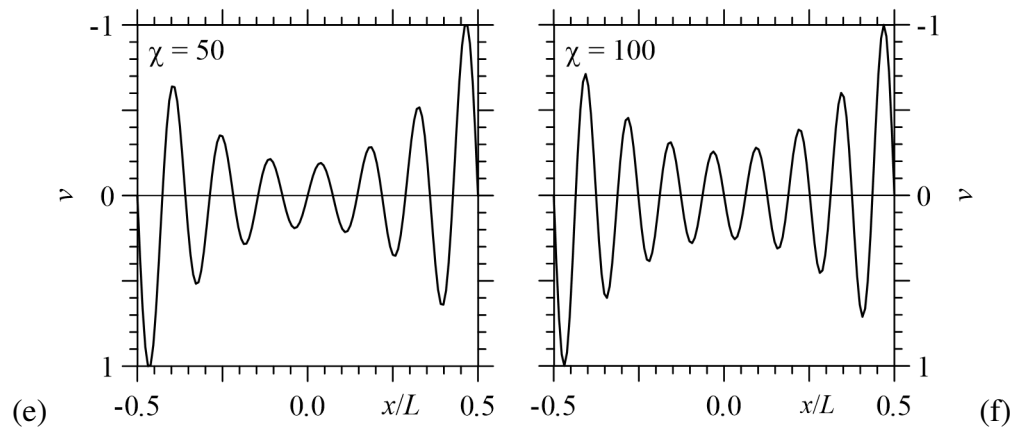
460



461



462



463

Fig. 11. Second mode shape for a beam with pinned ends,  $\alpha L = 50$  and increasing  $\chi$ .

464

#### 465 4.1 Influence of beam width on buckling wavelength

466

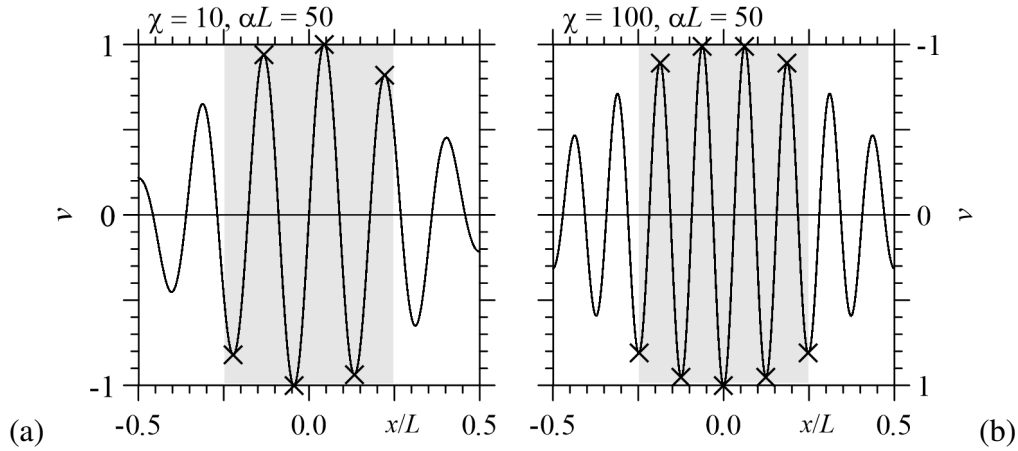
467

468

As stated into the introduction, the determination of buckling wavelength and amplitude of thin films on elastic substrates is important for stretchable and flexible electronics. Hence, the proposed numerical model is adopted for determining the critical buckling wavelength  $\Lambda_{cr}$  corresponding to



469  $P_{cr,s,1}$  for varying  $\alpha L$  and  $\chi$ . In order to avoid the local effect of the sliding ends,  $\Lambda_{cr}$  is evaluated  
 470 numerically as the average wavelength of the sinusoidal modal shape for  $-L/4 \leq x \leq L/4$  (Fig. 12).



471

472 Fig. 12. Determination of buckling wavelength corresponding to the minimum critical load for  
 473  $-L/4 \leq x \leq L/4$ , for two  $\alpha L$  and  $\chi$  cases.

474

475 Results are collected in Fig. 13a with cross symbols for several  $\chi$  values. The buckling  
 476 wavelength  $\Lambda_{cr}$  for each length-to-width ratio  $\chi$  turns out to decrease for increasing  $\alpha L$  and it  
 477 decreases for increasing  $\chi$ , as it can be noted in Fig. 12. However, for decreasing  $\chi$ ,  $\Lambda_{cr}$  values turn  
 478 out to be close to those of a beam on elastic half-plane  $\Lambda_{cr,2D}$  (dashed line in Fig. 13a). It is worth  
 479 noting that  $\Lambda_{cr,2D} = 9.97/\alpha = 2^{5/3}\pi/\alpha$ ; such expression can be derived analytically from Reissner  
 480 (1937) formulation, it was highlighted in Volynskii et al. (2000) and it was already obtained  
 481 numerically by authors for a beam with sliding ends on elastic half-plane (Tullini et al., 2013a).

482 It can be also noted that ratios  $\Lambda_{cr}/\Lambda_{cr,2D}$ , obtained with different  $\alpha L$  and  $\chi$  combinations with the  
 483 same ratio  $\alpha L/\chi$ , turn out to be very close to each other, and the same ratios can be obtained by  
 484 measuring the wavelength of the third and fourth modal shapes of a beam with pinned ends. Hence,  
 485 in order to obtain an approximated expression for  $\Lambda_{cr}$ , it is useful to introduce a function  $f(\alpha L/\chi) = f$   
 486  $(\alpha b)$ , representing the ratio between the buckling wavelength of a beam on elastic half-space and the  
 487 buckling wavelength of a beam on elastic half-plane:

488  $\Lambda_{cr} = \Lambda_{cr,2D} f(\alpha L / \chi)$  (23)

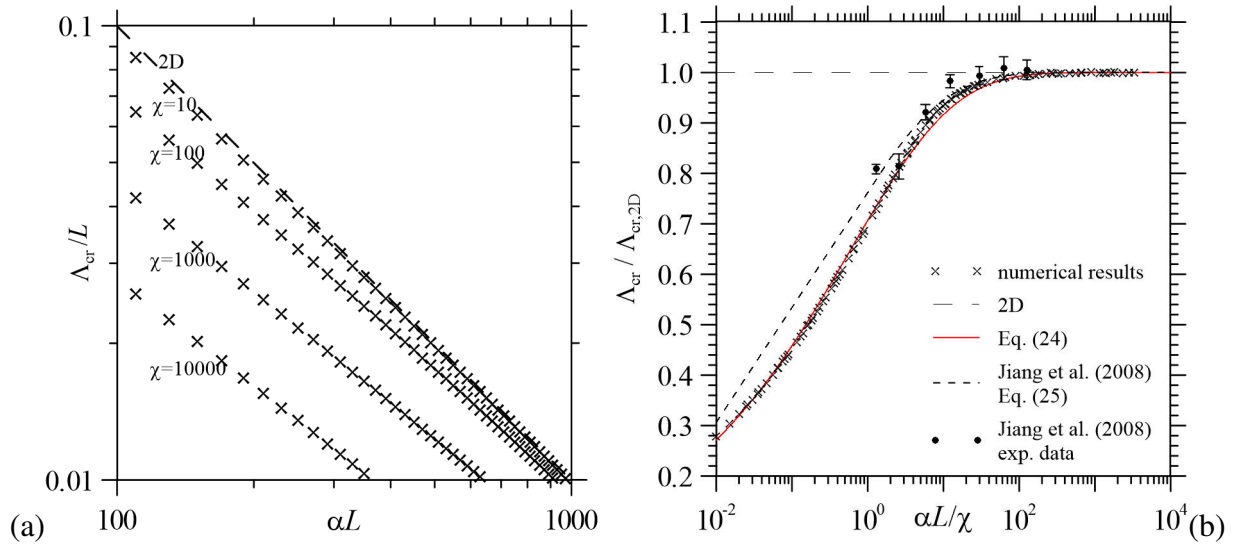
489 Ratios  $\Lambda_{cr} / \Lambda_{cr,2D}$  obtained numerically with the proposed model are shown in Fig. 13b versus  $\alpha b$   
 490 with cross symbols. It can be observed that the buckling wavelength values obtained with  $\alpha b$  larger  
 491 than  $10^3$  converge to those of a beam on elastic half-plane, since the corresponding ratios  
 492  $\Lambda_{cr} / \Lambda_{cr,2D}$  converge to 1.

493 A good approximation of the wavelength of beams on elastic substrate is given by the following  
 494 expression:

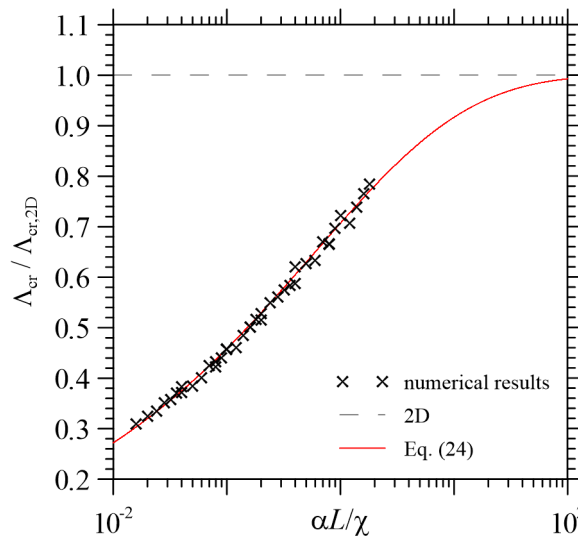
495  $\Lambda_{cr} = \Lambda_{cr,2D} \tanh[0.88(\alpha b)^{0.25}]$ , (24)

496 where the function  $f(\alpha L, \chi) = f(\alpha b) = \tanh[0.88(\alpha b)^{0.25}]$  is added with a red continuous line to  
 497 Fig. 13b versus  $\alpha b$ . Eq. (24) turns out to be similar, but not coincident, with that of a beam with  
 498 infinite length on half-space proposed by Jiang et al. (2008), which is in better agreement with their  
 499 experimental results (circles with error bar in Fig. 13b). The approximated expression for  $\Lambda_{cr}$  is  
 500 characterized by a coefficient of determination  $R^2$  close to 1 for almost all  $\alpha L$  and  $\chi$  combinations,  
 501 with the smallest  $R^2 = 0.77$  obtained with a beam having  $\chi = 100$  and varying  $\alpha L$  from 50 to 1000. It  
 502 is worth noting that the convergence of Eq. (24), for increasing  $\alpha b$ , to the analytical solution typical  
 503 of the plane state case, allows to consider such equation as a generalized approximated expression  
 504 for the critical wavelength of beams on an elastic continuum. It is worth noting that Euler-Bernoulli  
 505 beam model holds for sufficiently high values of the critical half-wavelength, for example,  
 506  $\Lambda_{cr}/2 > 10 h$ . Thus, making use of Eq. (24), the inequality  $\alpha h < f(\alpha b)/2$  holds. For beam with  
 507  $\alpha h > f(\alpha b)/2$ , the transverse shear deformation of the beam may become important and needs to be  
 508 considered. For the experimental data reported by Jiang et al. (2008), a Euler-Bernoulli beam model  
 509 may be adopted.

510 Finally, the buckling wavelength values of the modal shapes corresponding to  $P_{cr,p,2}$  (Fig. 11),  
 511 determined with the approach highlighted in Fig. 12 and compared with  $\Lambda_{cr,2D}$ , are shown in Fig. 14  
 512 for relatively small  $ab$  values, being in good agreement with Eq. (24) and justifying the  
 513 convergence of  $P_{cr,p,2}$  to  $P_{cr,s,1}$  for decreasing  $ab$ .  
 514



515 (a) 100  $\alpha L$  1000  
 516 Fig. 13. Buckling wavelength of beams with sliding ends on elastic half-space versus  $\alpha L$  and  
 517 varying  $\chi$  (a); with respect to the wavelength of a beam on elastic half-plane versus  $\alpha L/\chi$  (b).  
 518



519  
 520 Fig. 14. Buckling wavelength corresponding to  $P_{cr,p,2}$  with respect to the wavelength of a beam  
 521 on elastic half-plane versus  $\alpha L/\chi$ .

## 522 CONCLUSIONS

523 A simple and effective FE-BIE coupling method for beams on three-dimensional half-space,  
524 already investigated by authors by performing static analyses (Baraldi and Tullini, 2018), was here  
525 applied to buckling problems of slender beams and coatings having finite width and length, in  
526 bilateral and frictionless contact with an elastic half-space. Several beam end constraints were taken  
527 into consideration for simulating free coatings or different superstructures connected to a foundation  
528 beam. The proposed coupled FE-BIE model turned out to be fast and effective in evaluating beam  
529 buckling loads and the corresponding modal shape characteristics.

530 Considering a fixed beam length-to-width ratio  $\chi$  equal to 10, the buckling behaviour of a beam  
531 on elastic half-space turned out to be similar to that of a beam on elastic half-plane. On one hand,  
532 the proposed numerical tests showed a convergence, for low values of  $\alpha L$ , to the critical loads of  
533 beams without an elastic support. On the other hand, for increasing beam slenderness and/or  
534 substrate stiffness, a variation of the critical loads proportional to  $(\alpha L)^2$  was found, but  
535 dimensionless minimum critical loads were slightly larger than the corresponding ones typical of a  
536 beam on elastic half-plane (Tullini et al., 2013a). Furthermore, the beam with sliding ends showed a  
537 behaviour characterized by sinusoidal modal shapes over its length, which is typical of a beam with  
538 infinite length. The first and second dimensionless critical loads of the beam with pinned ends  
539 turned out to be slightly smaller than that obtained with the beam with sliding ends and the  
540 corresponding modal shapes were characterized by large amplitudes close to beam ends, whereas  
541 the third critical load converged to that of the beam with sliding ends, with sinusoidal modal shapes.

542 Focusing on the influence of beam width on beam buckling loads, a relationship between the  
543 dimensionless critical loads and the beam length-to-width ratio was also found and a new  
544 dimensionless parameter  $\alpha L/\chi = \alpha b$  was introduced for accounting to beam slenderness, width and  
545 half-space stiffness into a unique parameter. For increasing  $\alpha b$ , the first three dimensionless critical  
546 loads of a beam with pinned ends turned out to converge to the corresponding numerical solutions  
547 of a beam on elastic half-plane already obtained by Tullini et al. (2013a), where the third

548 dimensionless critical load is also in agreement with Reissner solution for the buckling of a beam  
 549 with infinite length (Biot, 1937), which is often adopted for describing the buckling of thin coatings  
 550 in plane strain conditions and to define the corresponding critical stresses.

551 Approximated expressions for fitting the numerical results were proposed for the first three  
 552 dimensionless critical loads of pin-ended beams and for the buckling wavelength of sliding-ended  
 553 beams, in order to obtain generalized formulas for estimating the minimum critical loads and the  
 554 critical wavelength of beams on an elastic continuum. In particular, the proposed expression for the  
 555 buckling wavelength turned out to be more accurate than existing analogous formulas and in  
 556 agreement with existing laboratory tests.

557 As a future challenging task, frictionless assumption will be removed to consider also tangential  
 558 tractions at the interface between the beam and the half-space boundary. In this case the task is  
 559 more burdensome than that outlined in Tezzon et al. (2015, 2016) for a beam in adhesive contact  
 560 with a half-plane. In fact, tangential and normal surface tractions are coupled with both horizontal  
 561 and vertical displacements.

## 562 **ACKNOWLEDGMENTS**

563 The present investigation was developed in the framework of the Research Program FAR 2021  
 564 of the University of Ferrara.

## 565 **APPENDIX**

566 For a generic  $i$ -th beam element, the stiffness matrix  $\tilde{\mathbf{K}}_{bi}$  is (Tullini et al. 2013a, Baraldi and  
 567 Tullini, 2018):

$$568 \quad \tilde{\mathbf{K}}_{bi} = \left( \frac{L}{l_{xi}} \right)^3 \begin{bmatrix} 12 & -6l_{xi} & -12 & -6l_{xi} \\ & 4l_{xi}^2 & 6l_{xi} & 2l_{xi}^2 \\ & & 12 & 6l_{xi} \\ \text{sym} & & & 4l_{xi}^2 \end{bmatrix}$$

569 Considering the penalty parameter  $k$  already introduced in section 2.1, in case of beam with sliding  
 570 ends, the stiffness matrices of the 1st and last beam elements become:

$$571 \quad \tilde{\mathbf{K}}_{b1} = \left(\frac{L}{l_{x1}}\right)^3 \begin{bmatrix} 12 & -6l_{x1} & -12 & -6l_{x1} \\ & 4l_{x1}^2 + k & 6l_{x1} & 2l_{x1}^2 \\ & & 12 & 6l_{x1} \\ \text{sym} & & & 4l_{x1}^2 \end{bmatrix}, \quad \tilde{\mathbf{K}}_{bn_x} = \left(\frac{L}{l_{xn_x}}\right)^3 \begin{bmatrix} 12 & -6l_{xn_x} & -12 & -6l_{xn_x} \\ & 4l_{xn_x}^2 & 6l_{xn_x} & 2l_{xn_x}^2 \\ & & 12 & 6l_{xn_x} \\ \text{sym} & & & 4l_{xn_x}^2 + k \end{bmatrix}.$$

572 Leading to a stiffness matrix for the entire beam as follows:

$$573 \quad \tilde{\mathbf{K}}_b = L^3 \begin{bmatrix} 12/l_{x1}^3 & -6/l_{x1}^2 & 12/l_{x1}^3 & -6/l_{x1}^2 & \cdots & 0 & 0 & 0 & 0 \\ -6/l_{x1}^2 & 4/l_{x1} + k & 6/l_{x1}^2 & -2/l_{x1} & \cdots & 0 & 0 & 0 & 0 \\ \vdots & \vdots & \vdots & \vdots & \vdots & \vdots & \vdots & \vdots & \vdots \\ 0 & 0 & 0 & 0 & \cdots & -6/l_{xn_x}^2 & 2/l_{xn_x} & 6/l_{xn_x}^2 & 4/l_{xn_x} + k \end{bmatrix}.$$

574 Whereas in case of beam with pinned ends, the stiffness matrix of the entire beam becomes:

$$575 \quad \tilde{\mathbf{K}}_b = L^3 \begin{bmatrix} 12/l_{x1}^3 + k & -6/l_{x1}^2 & 12/l_{x1}^3 & -6/l_{x1}^2 & \cdots & 0 & 0 & -k & 0 \\ \vdots & \vdots & \vdots & \vdots & \vdots & \vdots & \vdots & \vdots & \vdots \\ -k & 0 & 0 & 0 & \cdots & -12/l_{xn_x}^3 & 6/l_{xn_x}^2 & 12/l_{xn_x}^3 + k & 6/l_{xn_x}^2 \\ 0 & 0 & 0 & 0 & \cdots & -6/l_{xn_x}^2 & 12/l_{xn_x}^3 & 6/l_{xn_x}^2 & 4/l_{xn_x} \end{bmatrix}.$$

## 576 REFERENCES

- 577 Allen, H.G., 1969. Analysis and Design of Structural Sandwich Panels. Pergamon Press, Oxford.
- 578 Anyaegbunam, A.J., 2014. Complete stress and displacements in a cross-anisotropic half-space  
 579 caused by a surface vertical point load. Int. J. Geomech. 14(2), 171–181.
- 580 Argatov, I., Mishuris, G., 2018. Indentation Testing of Biological Materials. Springer, Cham.  
 581 <https://doi.org/10.1007/978-3-319-78533-2>
- 582 Baraldi, D., 2019. Static and buckling analysis of thin beams on an elastic layer. Comp. Mech.  
 583 Comput. Appl. Int. J. 10(3), 187–211.
- 584 Baraldi, D., Tullini, N., 2017. Incremental analysis of elastoplastic beams and frames resting on an  
 585 elastic half-plane. J. Eng. Mech. 143(9), 04017101, 1–9.

586 Baraldi, D., Tullini, N., 2018. In-plane bending of Timoshenko beams in bilateral frictionless  
587 contact with an elastic half-space using a coupled FE-BIE method. *Eng. Anal. Bound. Elem.*  
588 97, 114–130.

589 Baraldi, D., Tullini, N., 2020. Static stiffness of rigid foundation resting on elastic half-space using  
590 a Galerkin boundary element method. *Eng. Struct.* 225, 111061, 1–14.

591 Bielak, J., Stephan, E., 1983. A modified Galerkin procedure for bending of beams on elastic  
592 foundations. *SIAM J. Sci. Stat. Comput.* 4(2), 340–352.

593 Biot, M.A., 1937. Bending of an infinite beam on an elastic foundation. *J. Appl. Mech.* 4, A1–A7.

594 Bowden, N., Huck, W.T.S., Paul, K.E., Whitesides, G.M., 1999. The controlled formation of  
595 ordered, sinusoidal structures by plasma oxidation of an elastomeric polymer. *Appl. Phys.*  
596 *Lett.* 75(17), 2557–2559.

597 Davies, J.M., 2001. *Lightweight Sandwich Construction*. Blackwell Science, Oxford.

598 Ding, H., Chen, W., Zhang, L., 2006. *Elasticity of Transversely Isotropic Materials*. Springer,  
599 Dordrecht.

600 Erwin, V.J., Stephan, E.P., 1992. Adaptive approximations for 3-D electrostatic plate problems.  
601 *Adv. Eng. Software* 15(3–4), 211–215.

602 Falope, F.O., Lanzoni, L., Radi, E., 2020. Buckling of a Timoshenko beam bonded to an elastic  
603 half-plane: Effects of sharp and smooth beam edges *Int. J. Solids Struct.* 185–186, 222–239.

604 Gallagher, A.P., 1974. Buckling of a beam under axial compression with elastic support. *Stud.*  
605 *Numer. Anal.* 137–150.

606 Genzer, J., Groenewold, J., 2006. Soft matter with hard skin: from skin wrinkles to templating and  
607 material characterization. *Soft Matter* 2, 310–323.

608 Goodier, J.N., Hsu, C.S., 1954. Nonsinusoidal buckling modes of sandwich plates. *J. Aeronaut. Sci.*  
609 21, 525–532.

610 Gough, G.S., Elam C.F., de Bruyne, N.A., 1940. The stabilisation of a thin sheet by a continuous  
611 supporting medium. *J. R. Aeronaut. Soc.* 44, 12–43.

612 Graham, I.G., McLean, W., 2006. Anisotropic mesh refinement: the conditioning of Galerkin  
613 boundary element matrices and simple preconditioners. *SIAM J. Numer. Anal.* 44(4), 1487–  
614 1513.

615 Gurtin, M.E., Sternberg, E., 1961. Theorems in linear elastostatics for exterior domains. *Arch.*  
616 *Ration. Mech. Anal.* 8, 99–119.

617 Hetenyi, M., 1946. *Beam on Elastic Foundation*. University of Michigan Press, Michigan.

618 Huang, R., 2005, Kinetic wrinkling of an elastic film on a viscoelastic substrate. *J. Mech. Phys.*  
619 *Solids* 53(1), 63–89.

620 Huang, R., Suo, Z., 2002a. Instability of a compressed elastic film on a viscous layer. *Int. J. Solids*  
621 *Struct.* 39(7), 1791–1802.

622 Huang, R., Suo, Z., 2002b. Wrinkling of a compressed elastic film on a viscous layer. *J. Appl. Phys.*  
623 91(3), 1135–1142.

624 Jiang, H., Khang, D.Y., Fei, H., Kim, H., Huang, Y., Xiao, J., Rogers, J.A., 2008. Finite width  
625 effect of thin-films buckling on compliant substrate: Experimental and theoretical studies. *J.*  
626 *Mech. Phys. Solids* 56, 2585–2598.

627 Johnson, K.L., 1985. *Contact mechanics*. Cambridge University Press, Cambridge.

628 Kachanov, M.L., Shafiro, B., Tsukrov, I., 2003. *Handbook of elasticity solutions*. Kluwer Academic  
629 Publishers, Dordrecht. <https://doi.org/10.1007/978-94-017-0169-3>

630 Kerr, A.D., 1974. The stress and stability analyses of railroad tracks. *ASME J. Appl. Mech.* 41,  
631 841–848.

632 Kerr, A.D., 1978. Analysis of thermal track buckling in the lateral plane. *Acta Mech.* 30, 17–50.

633 Kerr, A.D., 1984. Shade, P.J., Analysis of concrete pavement blowups. *Acta Mech.* 52, 201–224.

634 Kikuchi, N., 1980. Beam bending problems on a Pasternak foundation using reciprocal variational-  
635 inequalities. *Q. Appl. Math.* 38(1), 91–108.

636 Kikuchi, N., Oden, J., 1988. *Contact problems in elasticity. A study of variational inequalities and*  
637 *finite element methods*. SIAM, Philadelphia.



- 638 Ley, R.P., Lin W., Mbanefo, U., 1999. Facesheet wrinkling in sandwich structures, NASA, CR-  
639 1999-208994, Virginia.
- 640 Liao, J.H., Wang, C., 1998. Elastic solutions for a transversely isotropic half-space subjected to a  
641 point load. *Int. J. Numer. Anal. Meth. Geomech.* 22, 425–447.
- 642 Lim, N.-H., Park, N.-H., Kang, Y.-J., 2003. Stability of continuous welded rail track. *Comp. Struct.*  
643 81, 2219–2236.
- 644 Marmo, F., Toraldo, F., Rosati, L., 2017. Transversely isotropic half-spaces subject to surface  
645 pressures. *Int. J. Solids Struct.* 104–105, 35–49.
- 646 Michell, J.H., 1900. The stress in an æolotropic elastic solid with an infinite plane boundary. *Proc.*  
647 *Lond. Math. Soc.* 32, 247–258.
- 648 Murthy, G.K.N., 1973. Buckling of continuously supported beams. *J. Appl. Mech.* 40(2), 546–552.
- 649 Popov, V.L., Heß, M., Willert, E., 2019. *Handbook of Contact Mechanics. Exact Solutions of*  
650 *Axisymmetric Problems.* Springer, Berlin. <https://doi.org/10.1007/978-3-662-58709-6>
- 651 Prager, W., 1927. Zur Theorie elastische gelagerter Konstruktionen. *Z. Angew. Math. Mech.* 7(5),  
652 354–360.
- 653 Reddy, J.N., 2006. *An Introduction to the Finite Element Method*, 3rd Ed. McGraw Hill, Singapore.
- 654 Reissner, M.E., 1937. On the theory of beams resting on a yielding foundation. *P. N. A. S.* 23(6),  
655 328–333.
- 656 Selvadurai, A.P.S., 1979a. *Elastic analysis of soil-foundation interaction.* Elsevier, *Developments in*  
657 *Geotechnical Engineering*, Amsterdam.
- 658 Selvadurai, A.P.S., 1979b. The interaction between a uniformly loaded circular plate and an  
659 isotropic elastic halfspace: a variational approach. *J. Struct. Mech.* 7(3), 231–246.
- 660 Selvadurai, A.P.S., 1980. Elastic contact between a flexible circular plate and a transversely  
661 isotropic elastic halfspace. *Int. J. Solids Struct.* 16, 167–176.
- 662 Selvadurai, A.P.S., 1984. A contact problem for a Reissner plate and an isotropic elastic halfspace.  
663 *J. Mech. Theor. Appl.* 3(2), 181–196.

664 Shield, T.W., Kim, K.S., Shield, R.T., 1994. The buckling of an elastic layer bonded to an elastic  
665 substrate in plane strain. *ASME J. Appl. Mech.* 61, 231–235.

666 Stafford, C.M., Harrison, C., Beers, K.I., Karim, A., Amis, E.J., Vanlandingham, M.R., Kim, H.C.,  
667 Volksen, W., Miller, R.D., Simonyi, E.E., 2004. A buckling-based metrology for measuring  
668 the elastic moduli of polymeric thin films. *Nat. Mater.* 3(8), 545–550.

669 Tarasovs, S. Andersons, J., 2008. Buckling of a coating strip of finite width bonded to elastic half-  
670 space. *Int. J. Solids Struct.* 45(2), 593–600.

671 Timoshenko, S.P., Gere, J.M., 1961. *Theory of Elastic Stability*. McGraw-Hill, New York.

672 Tezzon, E., Tralli, A., Tullini, N., 2018. Debonding of FRP and thin films from an elastic half-plane  
673 using a coupled FE-BIE model. *Eng. Anal. Bound. Elem.* 93, 21–28.

674 Tezzon, E., Tullini, N., Lanzoni, L., 2016. A coupled FE-BIE model for the static analysis of  
675 Timoshenko beams bonded to an orthotropic elastic half-plane. *Eng. Anal. Bound. Elem.* 71,  
676 112–128.

677 Tezzon, E., Tullini, N., Minghini, F., 2015. Static analysis of shear flexible beams and frames in  
678 adhesive contact with an isotropic elastic half-plane using a coupled FE-BIE model. *Eng.*  
679 *Struct.* 104, 32–50.

680 Tullini, N., Tralli, A., 2010. Static analysis of Timoshenko beam resting on elastic half-plane based  
681 on the coupling of locking-free finite elements and boundary integral. *Comput. Mech.* 45(2–  
682 3), 211–225.

683 Tullini, N., Tralli, A., Baraldi, D., 2013a. Stability of slender beams and frames resting on 2D  
684 elastic half-space. *Arch. Appl. Mech.* 83(3), 467–482.

685 Tullini, N., Tralli, A., Baraldi, D., 2013b. Buckling of Timoshenko beams in frictionless contact  
686 with an elastic half-plane. *J. Eng. Mech.* 139(7), 824–831.

687 Tullini, N., Tralli, A., Lanzoni, L., 2012. Interfacial shear stress analysis of bar and thin film bonded  
688 to 2D elastic substrate using a coupled FE-BIE method. *Finite Elem. Anal. Des.* 55, 42–51.

- 689 Vesic, A.B., 1961. Bending of beams resting on isotropic elastic solid. *J. Eng. Mech.* 87(2), 35–53.  
690 <https://doi.org/10.1061/JMCEA3.0000212>
- 691 Volynskii, A.L., Bazhenov, S., Lebedeva, O.V., Bakeev, N.F., 2000. Mechanical buckling  
692 instability of thin coatings deposited on soft polymer substrates. *J. Mater. Sci.* 35, 547–554.
- 693 Wang, C., Zhang, S., Nie, S., Su, Y., Chen, W., Song, J., 2020. Buckling of a stiff thin film on a bi-  
694 layer compliant substrate of finite thickness. *Int. J. Solids Struct.* 188–189, 133–140.
- 695 Wieghardt, K., 1922. Über den Balken auf nachgiebiger Unterlage. *Z. Angew. Math. Mech.* 2(3),  
696 165–184.
- 697 Wilder, E.A., Guo, S., Lin-Gibson, S., Faselka, M.J., Stafford, C.M., 2006. Measuring the modulus  
698 of soft polymer networks via a buckling-based metrology. *Macromolecules* 39(12), 4138–  
699 4143.
- 700 Winkler, E., 1867. *Die Lehre von der Elastizität und Festigkeit*. Dominicus, Prague.

701 **Figure captions**

702 Fig. 1. Compressed beam resting on a half-space.

703 Fig. 2. Beam with pinned ends on a half-space, given by a rigid frame with columns hinged to  
704 the foundation beam (a); beam with sliding ends on a half-space, given by a frame with rigid  
705 columns and simply supported beam (b).

706 Fig. 3. Relative differences for the first three critical loads versus the overall number  
707 subdivisions along beam length for a compressed beam with free ends with  $\alpha L = 5$  (a, c) and 25 (b,  
708 d), with  $\chi = 10$

709 Fig. 4. Dimensionless critical loads  $P_{cr,s}$  versus  $\alpha L$  for a beam with sliding ends on elastic half-  
710 space.

711 Fig. 5. First (continuous line) and second (dashed line) mode shapes for a beam with sliding ends  
712 and  $\alpha L$  equal to 5 (a) and 25 (b).

713 Fig. 6. Dimensionless critical loads  $P_{cr,p}$  versus  $\alpha L$  for a beam with pinned ends on elastic half-  
714 space.

715 Fig. 7. First (continuous line) and second (dashed line) mode shapes for a beam with pinned ends  
716 on half-space and  $\alpha L$  equal to 5 (a), 10 (b), 25 (c) and 50 (d).

717 Fig. 8. Dimensionless critical loads  $P_{cr,f}$  versus  $\alpha L$  for a beam with free ends on elastic half-  
718 space.

719 Fig. 9. First (continuous line) and second (dashed line) mode shapes for a beam with free ends  
720 and  $\alpha L$  equal to 1 (a), 5 (b), 10 (c) and 25 (d).

721 Fig. 10. First three dimensionless critical loads of a beam on half-space versus  $\alpha L/\chi$ .

722 Fig. 11. Second mode shape for a beam with pinned ends,  $\alpha L = 50$  and increasing  $\chi$ .

723 Fig. 12. Determination of buckling wavelength corresponding to the minimum critical load for  
724  $-L/4 \leq x \leq L/4$ , for two  $\alpha L$  and  $\chi$  cases.

725 Fig. 13. Buckling wavelength of beams with sliding ends on elastic half-space versus  $\alpha L$  and  
726 varying  $\chi$  (a); with respect to the wavelength of a beam on elastic half-plane versus  $\alpha L/\chi$  (b).

727 Fig. 14. Buckling wavelength corresponding to  $P_{cr,p,2}$  with respect to the wavelength of a beam  
728 on elastic half-plane versus  $\alpha L/\chi$ .

729 **Table captions**

730 Tab. 1. Reference critical loads for a compressed beam with free ends on elastic half-space,  
731 obtained with  $n_x = 2^{11}$  and a power-graded subdivision along y direction with  $n_y = 7$  and  $\beta = 3$ .

732 Tab. 2. Dimensionless critical loads of a beam on half-space with  $\alpha L = 50$  varying  $\chi$ .